Neuron
Article

Precursor Diversity and Complexity of Lineage Relationships in the Outer Subventricular Zone of the Primate

Marion Betizeau,[1,2] Veronique Cortay,[1,2] Dorothée Patti,[1,2] Sabina Pfister,[3] Elodie Gautier,[1,2] Angèle Bellemin-Ménard,[1,2] Marielle Afanassieff,[1,2] Cyril Huissoud,[1,2,4] Rodney J. Douglas,[3] Henry Kennedy,[1,2] and Colette Dehay[1,2,*]
[1]Stem Cell and Brain Research Institute, INSERM U846, 18 Avenue Doyen Lepine, 69500 Bron, France
[2]Université de Lyon, Université Lyon I, 69003 Lyon, France
[3]Institute of Neuroinformatics (INI), Winterthurerstrasse 190, University/ETH Zürich, CH-8057 Zürich, Switzerland
[4]Service de gynécologie-obstétrique, Hôpital de la Croix-Rousse, Hospices Civils de Lyon, 69004 Lyon, France
*Correspondence: colette.dehay@inserm.fr
http://dx.doi.org/10.1016/j.neuron.2013.09.032

SUMMARY

Long-term ex vivo live imaging combined with unbiased sampling of cycling precursors shows that macaque outer subventricular zone (OSVZ) includes four distinct basal radial glial (bRG) cell morphotypes, bearing apical and/or basal processes in addition to nonpolar intermediate progenitors (IPs). Each of the five precursor types exhibits extensive self-renewal and proliferative capacities as well as the ability to directly generate neurons, albeit with different frequencies. Cell-cycle parameters exhibited an unusual stage-specific regulation with short cell-cycle duration and increased rates of proliferative divisions during supragranular layer production at late corticogenesis. State transition analysis of an extensive clonal database reveals bidirectional transitions between OSVZ precursor types as well as stage-specific differences in their progeny and topology of the lineage relationships. These results explore rodent-primate differences and show that primate cortical neurons are generated through complex lineages by a mosaic of precursors, thereby providing an innovative framework for understanding specific features of primate corticogenesis.

INTRODUCTION

Besides its tangential expansion, one hallmark of human and nonhuman primate cortex is the selective enlargement of the supragranular layer compartment (Marín-Padilla, 1992), which is considered to underlie the highly developed computational abilities of the human brain (Kennedy et al., 2007). The enlarged supragranular primate layers originate from a specialized precursor pool, the outer subventricular zone (OSVZ) (Dehay et al., 1993; Lukaszewicz et al., 2005; Smart et al., 2002). Maximum dimensions of the OSVZ coincide with peak rates of supragranular neuron production (Fietz et al., 2010; Hansen et al., 2010; Smart et al., 2002).

The enlargement and complexification of the OSVZ is considered to be a key factor underlying evolutionary adaptive changes of primate corticogenesis, in turn leading to the structural characteristic and by consequence the functional dynamics of the primate neocortex (Dehay and Kennedy, 2007). A well-defined strategy to better understand the mechanisms leading to the evolutionary expansion of the primate cortex involves characterizing cortical progenitors (Fietz et al., 2010; Hansen et al., 2010; Lui et al., 2011).

Two principal cortical precursor types have been reported in primates and nonprimates: (1) apical progenitors (APs) undergoing mitosis at the ventricular surface in the ventricular zone (VZ) and (2) basal progenitors (BPs) undergoing mitosis at abventricular locations in the ISVZ and OSVZ. In rodents, APs comprise neuroepithelial cells, which transform into the apical radial glial (RG) cells of the VZ at the onset of neurogenesis (Götz and Huttner, 2005) and short neural precursors (Stancik et al., 2010). Rodent BPs include intermediate progenitor (IP) cells and rare basal (or outer) radial glial (bRG) cells, the latter accounting for less than 5% of the BP population (Martínez-Cerdeño et al., 2012; Shitamukai et al., 2011; Wang et al., 2011). In contrast to IP cells, which undergo one terminal round of cell division, bRG cells are competent to undergo up to two rounds of division (Shitamukai et al., 2011; Wang et al., 2011).

Several studies (Bystron et al., 2008; Fietz et al., 2010; García-Moreno et al., 2012; Hansen et al., 2010; Kelava et al., 2012; LaMonica et al., 2012; Levitt et al., 1981) have shown that the human and nonhuman primate BPs of the OSVZ include a large fraction of bRG cells. An unexpected feature of primate BPs is that the maintenance of radial glial-like morphology is accompanied by the expression of the transcription factor Pax6 (Fietz et al., 2010; Fish et al., 2008), as well as various combinations of stem cell markers such as Sox2 and Hes1 (Lui et al., 2011), further reinforcing the similitude of the primate bRG cells to the APs (Englund et al., 2005; Götz and Huttner, 2005). In addition, like APs, primate bRG cells have a long basal process, connecting the basal membrane at the pia, but they supposedly differ from APs by being devoid of apical process and undergo basally directed mitotic somal translocation (Fietz et al., 2010; Hansen et al., 2010).

The mechanisms responsible for the large increase of the BP pool in the primate are the subject of sustained speculations (Lui et al., 2011). During evolution, there is an increase in the number of bRG cells (Fietz et al., 2010; Reillo et al., 2011), reported to undergo up to two rounds of division in human (Hansen et al., 2010; LaMonica et al., 2013). The prevailing theory is that the expansion of the BP pool is ensured by transit-amplifying daughter progenitors (TAPs). It is further hypothesized that the TAPs undergo numerous symmetric divisions before differentiating into neurons. According to this theory, the TAPs ensure the massive increase in neuronal production that characterizes the primate cortex and contribute to its increased size and complexification (Fietz et al., 2010; Kriegstein et al., 2006; Lui et al., 2011; Martínez-Cerdeño et al., 2006; Pontious et al., 2008).

Here, using a combination of real-time imaging of individual precursors from long-term organotypic slice culture of embryonic macaque monkey and immunohistochemistry, we establish a detailed description of the proliferative behavior, morphology, and lineage relationships of OSVZ precursors. Using an unbiased sampling of cycling precursors, we have identified five distinct OSVZ precursor types, showing distinctive behavioral attributes. Besides the already described basal process-bearing bRG (bRG-*basal-P*) cells and IP cells (Fietz et al., 2010; Hansen et al., 2010), we have identified three distinct categories of bRG cells that include (1) apical process-bearing bRG (bRG-*apical-P*) cells, (2) apical and basal process bearing bRG cells (bRG-*both-P*), and (3) bRG cells alternating between stages showing either an apical and/or a basal process and stages with no process designed as transient bRG (tbRG) cells. Each precursor type undergoes numerous successive rounds of proliferative divisions. This extensive proliferation of OSVZ precursors is accompanied by cell-cycle duration of the same order as that observed in the VZ, with a significant shortening during the production of supragranular layer neurons. This contrasts with the progressive increase in cell-cycle duration reported in rodent corticogenesis (Caviness et al., 1995; Reznikov and van der Kooy, 1995).

The quantitative analysis of a large database of complex lineage trees generated by OSVZ precursors provided a powerful insight into rules governing precursor proliferative behavior and fate. State transition analyses of the lineage trees reveal frequent bidirectional transitions between precursor types. All five precursor types self-renew and directly generate neurons. Comparison of early and late stages of corticogenesis indicates a change in the topology of the precursor state transition diagram.

These results indicate a higher level of complexity in both the identity and in the lineage relationships of OSVZ precursors than previously reported (Fietz et al., 2010; Hansen et al., 2010) and predicted (Lui et al., 2011; Martínez-Cerdeño et al., 2006; Pontious et al., 2008).

The present study points to rodent-primate differences in precursor diversity and proliferative abilities, combined with species-specific tempo of cell-cycle regulation, having a profound impact on the phenotype of the adult cortex in these two orders. We propose that these specific properties of primate OSVZ precursors account for the observed expansion of the cortex and the supragranular layer enlargement.

RESULTS

OSVZ and Pax6/Tbr2 Expression

We provide a comprehensive description of the VZ, ISVZ, and OSVZ in presumptive area 17 covering the period of neurogenesis between embryonic day 49 (E49) and E94, (Figure 1) (Rakic, 1974). Cortical neuron production starts at E45 and BPs are first observed at E49 when they form the SVZ, which, compared to the VZ, exhibits a looser and sparser cell arrangement and includes a higher proportion of Tbr2+ precursors (Figure 1A). The OSVZ can be distinguished from the ISVZ at E58 and is characterized by compact and elongated precursors reminiscent of the VZ and distinct from the much looser disorganized appearance of the rodent SVZ (Lukaszewicz et al., 2005; Smart et al., 2002) (Figure 1B). In the occipital cortex, the OSVZ is basally bordered by an outer fiber layer (OFL) and undergoes rapid expansion to become the predominant germinal zone (GZ) at E63 before proceeding to decline after E78, some 15 days after the decline of the VZ (Figures 1C–1F). Quantification of the numbers of Ki67+ cells within the full thickness of the GZ shows that while the VZ is the major source of precursors prior to E58, as early as E63 the OSVZ becomes the prominent precursor pool (Figure 1G). From E70 there is a sharp drop in the proportions of cycling precursors in all compartments (Figure 1H).

Cycling precursors (Ki67+) express Pax6 and/or Tbr2 in a compartment-specific pattern (Figures 1A–1F and 1I). In the VZ and up to E79, 60%–80% of precursors express uniquely Pax6 (Pax6+ only cells). After E79, 40% of VZ precursors coexpress Pax6/Tbr2 and Tbr2+ only cells are rare. In the ISVZ, 60% to 80% of precursors coexpress Pax6/Tbr2, 5%–30% are Tbr2+ only and less than 15% are Pax6+ only cells. In the OSVZ, 25%–50% of precursors coexpress Pax6/Tbr2, 20% to 35% are Pax6+ only, 10%–20% are Tbr2+ only. Hierarchical clustering was used to explore the closeness/dissimilarity of the Pax6/Tbr2 expression patterns of the three GZ. On this basis, ISVZ and OSVZ appear more closely related with each other than with the VZ, and the early VZ is set apart as is the late OSVZ (Figures 1I and 1J).

OSVZ Precursors Undergo Multiple Rounds of Proliferative Divisions and Show Unusual Temporal Regulation of Cell-Cycle Parameters

Although the object of numerous speculations (Hansen et al., 2010; Kriegstein et al., 2006; Lui et al., 2011), the extent to which there is an expansion of OSVZ precursor pool has not been directly analyzed.

We have established optimal conditions for organotypic culture of monkey embryonic cortex (from E48 to E80), where tissue integrity is maintained for up to 15 days and where proliferation, migration to the cortical plate, and neuronal differentiation are conserved (Lukaszewicz et al., 2005) (Figures S1A–S1E; Movie S1 available online). Using two-photon time-lapse videomicroscopy (TLV), we recorded 487 divisions in 1,071 EGFP-expressing cells labeled via EGFP retroviral infection on parasagittal E48, E65, and E78 organotypic slices, corresponding to infragranular and supragranular layer production, respectively.

We reconstructed lineage trees containing three or more cells by playing back the video recordings frame by frame and

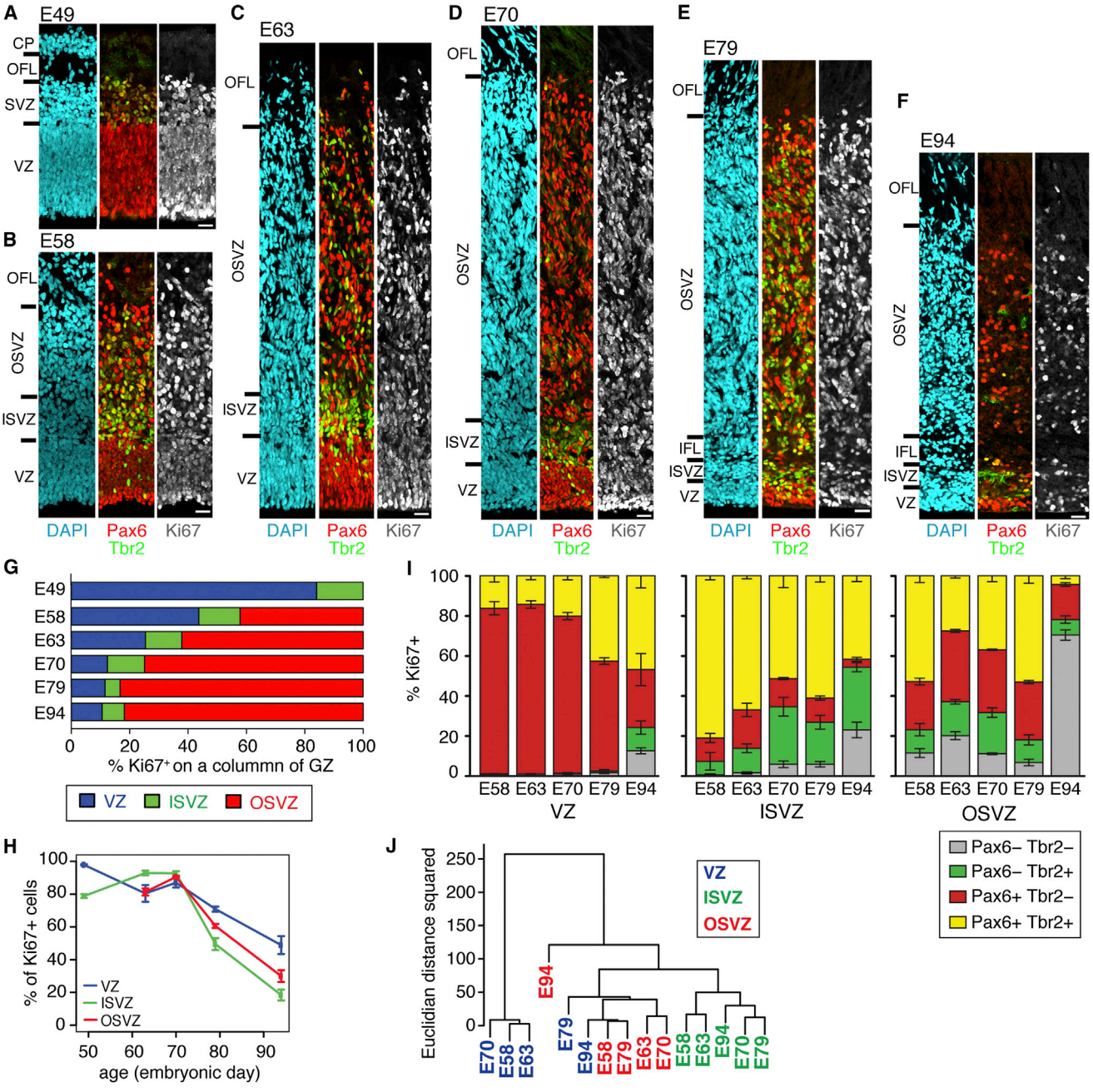

Figure 1. Germinal Zone-Specific Patterns of Pax6/Tbr2 Expression

(A–F) Microphotographs of parasagittal transects of Pax6/Tbr2/Ki67 immunostained visual cortex GZ from E49 to E94 (A, E49; B, E58; C, E63; D, E70; E, E79; and F, E94). Scale bar, 20 μm. VZ, ventricular zone; SVZ, subventricular zone; IFL, inner fiber layer; ISVZ, inner SVZ; OFL, outer fiber layer; OSVZ, outer SVZ; CP, cortical plate.

(G) Distribution of cycling precursors in each GZ during cortical neurogenesis.

(H) Proportion of Ki67+ precursors in VZ, ISVZ, and OSVZ at different stages (mean ± SEM; n = 3–4 representative transects per age, >500 cells counted per group).

(I) Proportions of Ki67+ progenitors expressing Pax6 and/or Tbr2 in VZ, ISVZ, and OSVZ (mean ± SEM; n = 3–4 representative images per stage, >500 cells counted per zone for each age).

(J) Hierarchical clustering of the GZ compartments. The proportions of each precursor type presented in (I) were transformed into a Euclidian distances matrix and subjected to a hierarchical clustering using Ward's minimum variance method.

mapping the birth order of the cells within each lineage. OSVZ precursors underwent up to six multiple rounds of proliferative divisions, allowing reconstruction of 91 lineage trees at E65 and E78 (Figure 2A; Movie S2). Compared to E65, E78 OSVZ precursors generated significantly more complex and extensive trees (Figure 2A). These stage-specific differences in

proliferative behavior were consistently observed across four E65 and two E78 hemispheres. The smaller size of E65 OSVZ trees (not exceeding three ranks with no division observed beyond 160 hr of recording; Figure 2A) was not due to experimental conditions in the monitoring period since at E65, on the same slices used for the OSVZ, divisions in the VZ were observed over five ranks and 200 hr of recording (Figure S1F). Comparison of the depth of lineage trees (number of successive divisions) revealed that OSVZ precursors generate longer lineage trees at E78 compared to E65 (Figure 2B). No significant difference was observed between VZ and OSVZ at either E65 or E78 (Figure 2B; Figure S1F).

Based on daughter cell fate, we defined a proliferative division when a precursor gives rise to two daughter cells, both of which undergo further division. Differentiative divisions occur when a progenitor gives rise to at least one daughter that exits the cell cycle. Compared to E65, E78 OSVZ and VZ precursors undergo significantly higher proportions of proliferative divisions (Figure 2C).

From the TLV recordings, we extracted cell-cycle durations (Tc)—defined as the time elapsed between two mitoses. VZ precursors show a mean Tc of 45 hr at E48 (n = 14) increasing up to 63 hr at E65 (n = 52) prior to shortening to 46 hr at E78 (n = 84) (Figure 2D). Tc variation in OSVZ follows the same time course as in the VZ. The longer Tc at early stages and shorter Tc at late stages were confirmed by similar results obtained from different brains at E63, E64, and E65, as well as in two E78 brains. OSVZ precursors cycle slightly but significantly slower than VZ precursors (Figure 2D).

Interestingly, the shorter Tc values observed in VZ and OSVZ at E78 are associated with increased proportions of proliferative divisions (Figure 2C), pointing to an upsurge in proliferative activity and coinciding with maximum tree size at this stage (Figure 2B). So as to quantify the dynamics of mode of division in vivo, we estimated the changes in rates of cell-cycle exit. NeuN immunoreactivity is selectively detected in postmitotic neurons of the subplate and cortical plate in the mouse and is a marker of neuronal differentiation (Wang et al., 2011). We observed low but significant levels of nuclear NeuN in a fraction of cycling precursors in the primate GZ (Figures S1G and S1H) (Lui et al., 2011). Hence, we used the percentage of Ki67+ NeuN+ double-positive cells with respect to the total cycling population as an index of the rate of cell-cycle exit (Figure 2E). In the VZ, the cell-cycle exit fraction increases slightly between E48 and E65 and decreases between E65 and E78. In the OSVZ/ISVZ, the cell-cycle exit fraction increases slightly between E48 and E70 before declining abruptly. At E78 in both the VZ and the OSVZ, compared to proliferative divisions, differentiative divisions showed significantly longer Tc values (52.3 hr versus 44.6 hr, 17% increase, Figure 2F).

The above analysis at the single-cell level has been complemented by an in situ population analysis of the relative duration of cell-cycle phases, using a triple immunolabeling against PCNA, Ki67, and Geminin (Figure 2G). In the VZ, the proportion of G1 phase cells increases from E48 to E65 and is associated with a decrease in the proportion of S phase precursors (Figure 2H), suggesting a relative lengthening of the G1 phase (TG1) and a relative shortening of S phase (TS). In the OSVZ, G1 cells accounted for 65% of the total cycling precursor pool at both E65 and E78, which is inferior to the proportions observed in the VZ at similar stages (80%), suggesting that OSVZ precursors have a relatively shorter TG1 than their VZ counterparts.

Using Tc values obtained with TLV, we estimated the theoretical duration of cell-cycle phases in the different compartments (Figure 2I). This analysis reveals that the Tc decrease between E65 and E78 is largely due to a reduction in TG1 and to a lesser extent in TS in the VZ. In the OSVZ, the Tc decrease between E65 and E78 results from a reduction of both TG1 and TS. Interestingly, this shortening in TG1 at E78 in both VZ and OSVZ is associated with an increase in proliferative divisions (Figure 2C).

The OSVZ Includes Five Precursor Types, a Fraction of which Shows a Dynamic Morphology

The maintenance of Pax6 expression in OSVZ precursors (Figure 1) (Fietz et al., 2010; Fish et al., 2008; Hansen et al., 2010), combined with the present findings of their extensive proliferative abilities, raises the question of the extent to which OSVZ precursors resemble VZ precursors.

Immunohistochemistry analysis performed a few days after EGFP retroviral infection showed that over 75% of OSVZ Ki67+ precursors correspond to radial-oriented cells (Figures 3A–3F; Figures S2A–S2J), which we broadly classify as bRG cells, 25% to nonpolarized IP precursors (Figure 3G; Figures S2K–S2N), and less than 1% to tangentially oriented precursors (Figure S2O). Data in Figure 3H represent the pooled results of the two ages. (Note that when no significant difference was observed between the two stages, results are pooled and age is not specified.)

We observed three different static bRG morphologies: (1) 40% of bRG cells bear an extensive basal process (bRG-*basal-P*), sometimes reaching the pia (Figures 3A and 3B; Figures S2A–S2C); (2) 10% of bRG cells bear a well-developed apical process (bRG-*apical-P*), extending as far as the ISVZ and VZ, without however reaching the ventricular surface (Figures 3C and 3D; Figure S2D); and (3) 50% of bRG cells bear both an apical and a basal process (bRG-*both-P*) (Figures 3E and 3F; Figures S2E–S2J). Hence, 60% of bRG cells exhibit an apical process (Figure 3I).

Immunohistochemistry combining EGFP, Ki67, Tbr2, and Pax6 showed that all three bRG types were predominantly Tbr2-Pax6+ and differed significantly from IP cells that were predominantly Tbr2+Pax6+ (Figure 3J). EGFP immunolabeling provides a high resolution, allowing detailed morphometric analysis of the precursor processes. This showed that thick basal processes are more frequent than thick apical processes (Figure 3K). The apical process is more likely to be thick when belonging to a bRG-*apical-P* cell rather than to a bRG-*both-P* cell, whereas frequency of basal thick processes is equivalent in bRG-*basal-P* and bRG-*both-P* cells. Basal processes are significantly longer than apical processes (Figure 3L).

TLV recordings showed that, while OSVZ precursors do not undergo interkinetic nuclear migration observed in VZ precursors, 24% of bRG cells undergo a mitotic translocating movement prior to mitosis (MST; Figure 3M). MST was observed to be basally (upward) as well as apically (downward) directed (Figure 3N). Note that MST is exclusively downward in bRG-*apical-P*

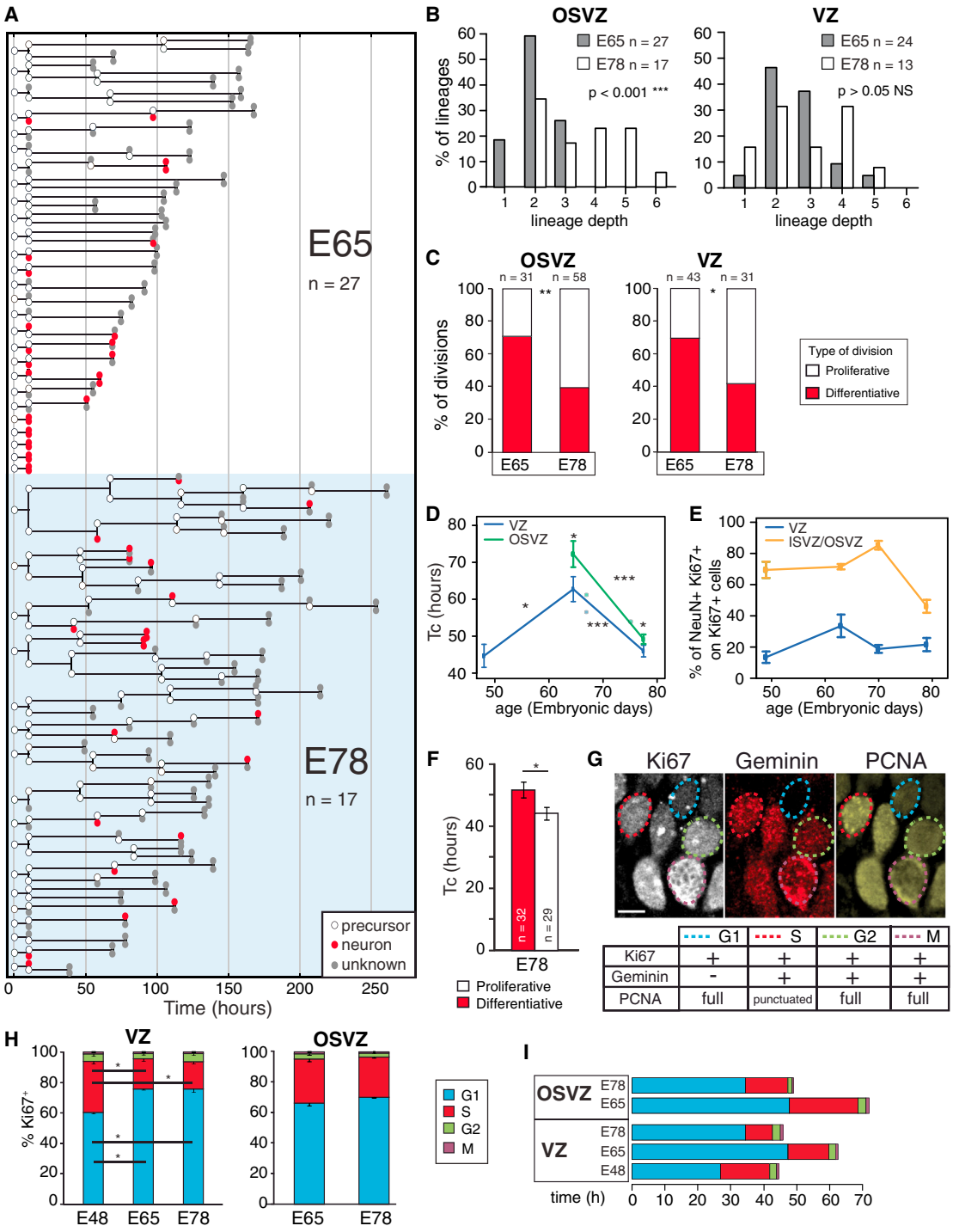

Figure 2. OSVZ Precursor Extensive Proliferative Abilities and Temporal Regulation of Cell-Cycle Parameters

(A) Ex vivo reconstruction of lineage trees. Summary of 44 representative lineage trees reconstructed from TLV in the OSVZ (E65: four hemispheres, ten slices; E78: two hemispheres, three slices).

(B) Distribution of the depth (number of successive divisions) of the OSVZ and VZ lineages shown in (A) and Figure S1F. Fisher's exact test.

(C) Frequency of proliferative and differentiative divisions in OSVZ and VZ at E65 and E78 (E65: four hemispheres, ten slices; E78: four hemispheres, ten slices). *$p < 0.05$, **$p < 0.01$ Fisher's exact test.

(D) Comparison of Tc between VZ and OSVZ (mean ± SEM, E48: n = 14 VZ; E65: n = 52 VZ, n = 40 OSVZ; E78: n = 84 VZ, n = 133 OSVZ, four hemispheres, ten slices per stage, except E48 [two hemispheres, four slices]). Dots represent sparse data at intermediate stages (E67, one hemisphere, one slice and E75, one hemisphere, two slices). *$p < 0.05$, ***$p < 0.001$ Wilcoxon test.

(legend continued on next page)

cells and upward in bRG-*basal-P* cells, while bRG-*both-P* cells and tbRG cells undergo equal proportions of downward and upward MST. MST amplitude ranges from 10 to 50 μm (Figure 3O) (the average diameter of precursors is 10 μm).

TLV observations confirmed the existence of IPs, bRG-*apical-P*, bRG-*basal-P*, and bRG-*both-P* cells as four distinct categories of precursors that exhibit a constant morphology throughout their lifetime—defined as the interval between two successive mitoses (see upper cell in Figure 4A and Movie S3 for an example of a bRG-*basal-P* cell, Movie S4 and Figure 4B for an IP). Unexpectedly, TLV observations revealed the existence of a fifth precursor type corresponding to precursors alternating between stages showing either an apical and/or a basal process and stages with no process (i.e., IP morphology) during at least 15% of their lifetime (Figure 4C; Figure S3A; lower daughter, Movie S5). This fifth type was designated as transient bRG (tbRG) cells.

In addition to morphology changes in tbRG cells, we also observed a certain degree of remodeling of the processes in bRG-*both-P* cells. Only 10% of bRG-*both-P* cells are born with the two processes and, in most cases, the newborn bRG-*both-P* cell grows a second process shortly after birth and exhibits the two processes during the major part of its lifetime (Figure 4A, lower cell; Figures S3B and S3C; upper daughter, Movie S5). In a few cases, bRG-*apical-P* cells (20%) and bRG-*basal-P* cells (14%), in addition to the continuous presence of their defining process, exhibit an additional short-lived temporary process.

Because a fraction of bRG cells exhibit dynamic processes, it was necessary to establish a reliable identification criterion defining the overall morphology throughout the precursor's lifetime. We observed that the morphology at mitosis correlates well with the morphology after birth and throughout the lifetime of the precursor (Figure 4D). Hence, the morphology observed under TLV before division was used to define bRG cell identity.

Given that cells are rounding up during mitosis, TLV analysis of the morphology right before mitosis is likely to be more accurate than the classically used phosphovimentin (an RG cell-specific mitotic marker) labeling to detect process-bearing precursors (Figure S3D). This is borne out by TLV observations, which, compared to phosphovimentin labeling, revealed lower proportions of dividing precursors devoid of process and higher proportions of mitotic bRG-*apical-P* cells and bRG-*both-P* cells (Figure 4E). This is in agreement with observations using phosphovimentin that report that when RG cells round up to divide, the basal process becomes extremely thin and forms small varicosities (Weissman et al., 2003). Because the apical process is significantly thinner than the basal process (Figure 3K), it may fail to be detected by phosphovimentin immunolabeling. Alternatively, vimentin may be expressed at low levels in the apical process.

Comparisons of the proportions of the five precursor types show that bRG-*both-P* cells and tbRG cells predominate at 25%, followed by bRG-*apical-P* cells (20%), and IP and bRG-*basal-P* cells correspond to the least numerous cell type at just under 15% each (Figure 4F).

Inheritance of Processes in OSVZ Precursors Is Determined by Horizontal Plane of Division and Affects Precursor Fate

Because morphology at mitosis is a good indicator of the morphology after birth and throughout the lifetime of a precursor (Figure 4D), we used morphology at mitosis to assess the inheritance of the basal or apical process as well as its influence on the fate of the progeny.

Analysis of the paired daughter cells generated by the different bRG cell morphotypes takes into account: (1) bRG mother cell morphology prior to mitosis, (2) morphology of the two daughter cells immediately following division, i.e., at birth, and (3) the relative position of each daughter cell after mitosis (upper basal or lower apical) (Figures 5A and 5B). This revealed that different bRG cell types differ in their paired daughter cell progeny and points to general rules of process inheritance.

In 80% of divisions of bRG-*both-P* cells, the basal process is inherited by the upper and the apical process by the lower daughter. In virtually all cases, the lower daughter of bRG-*apical-P* mother cells inherits the apical process and the upper daughter of bRG-*basal-P* the basal process. No upper daughter of a bRG-*basal-P* mother cell was found with an apical process confirming previous observations (Hansen et al., 2010; LaMonica et al., 2013).

These findings suggest a simple rule of process inheritance based on the position of the daughter cell. Further, TLV showed that the vast majority of bRG cells exhibit a horizontal cleavage plane (>80%; Figure 5C). Horizontal plane of division was also predominant in vivo at E78 (Figure 5D). The higher proportion of horizontal divisions at E65 observed on organotypic slices are likely due to the known influence of culture leading to increases in horizontal planes (Haydar et al., 2003; Konno et al., 2008).

We next examined how the inheritance of a given process at birth influences the identity of the precursor type (Figure 5E). We observed that cells born either with an apical or a basal process are prone to become cycling bRG cells (with a predominance for maintaining the inherited process) and to a lesser extent tbRG cells, whereas cells born without a process acquire a tbRG or IP cell phenotype.

This analysis reveals that bRG-*apical-P* corresponds mostly to lower daughters (79.3%), whereas bRG-*basal-P* corresponds to upper daughters (94.7%). Interestingly, Tc of sister daughters that both divide again are correlated and show a certain degree

(E) Cell-cycle exit rate estimated by the percentage of Ki67+/NeuN+ precursors (mean ± SEM; n = 3–4 representative images per age, >500 cells counted per group).
(F) Tc of proliferative versus differentiative divisions at E78 (mean ± SEM) *p < 0.05 Wilcoxon test.
(G–I) Cell-cycle kinetics vary between the different GZ. (G) Identification of the different phases of the cell-cycle using PCNA, Geminin, and Ki67 immunolabeling. Scale bar, 5 μm. G1 phase cells are Ki67+ Geminin−. Other phases are labeled by Geminin. S phase cells display punctuate PCNA staining. G2 cells are round, slightly bigger with homogeneous PCNA staining. M phase cells correspond to mitotic figures. (H) Proportions of precursors in the different cell-cycle phases in VZ and OSVZ (mean ± SEM; three to six representative GZ transects per age, >500 cells counted per group). *p < 0.05 Kruskal-Wallis test. (I). Length of the individual cell-cycle phases estimated from the proportions of precursors in each phase with respect to Tc measured with TLV in each zone. See also Figure S1.

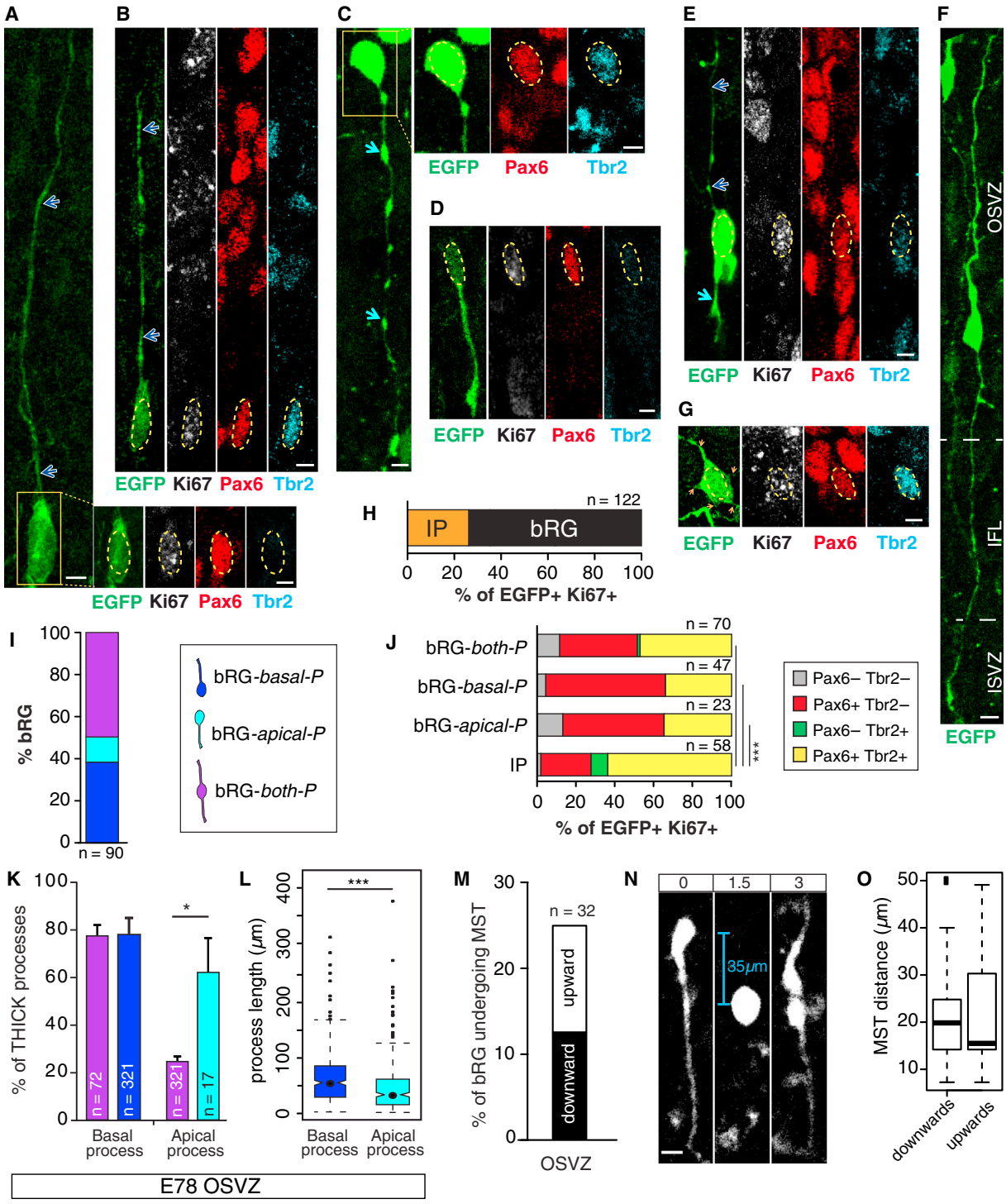

Figure 3. OSVZ Precursors Show an Unexpected Degree of Morphological and Molecular Diversity

(A–G) Examples of the different morphotypes of OSVZ EGFP+ precursors on organotypic slices immunostained for EGFP/Ki67/Pax6/Tbr2 after 3 to 6 days in vitro after EGFP retroviral infection at E78. Scale bar, 5 μm. (A and B) bRG with only a basal process are referred to as bRG-*basal-P* (basal process length > 100 μm in (A), dark blue arrowheads). Note that the bRG-*basal-P* in (A) expresses Pax6 but not Tbr2, whereas the *bRG-basal-P* in (B) expresses both markers. (C and D) bRG cells bearing a well-developed apical process referred to as bRG-*apical-P* (length > 100 μm in C, cyan arrowheads). Both cells express Pax6 but only the bRG in (C) expresses Tbr2. (E and F) bRG bearing both an apical and a basal process referred to as bRG-*both-P*. The two processes have different thicknesses (see K). The apical process of (F) extends as far as the ISVZ and basal VZ. (G) Multipolar cell with five processes (orange arrowheads) expressing both Pax6 and Tbr2.

(legend continued on next page)

of synchronization with that of the mother cell (Figures 5F and 5G). We failed to detect any effect of the relative upper or lower position of the two daughter cells on their neuron versus precursor fate (data not shown).

Stage-Specific Differences in Progeny and Lineage Relationships of the Five OSVZ Precursor Types

We have extracted quantitative information regarding the precursor fate by a clonal analysis of a database including 695 cells and 306 divisions at E65 and E78 (Figure S4A). This established distinctive stage-specific proliferative, self-renewing, and neurogenic characteristics for the five precursor types.

The five precursor types exhibit marked statistical differences in their order of apparition in the lineage trees. At E78, bRG-*both-P* cells and bRG-*basal-P* cells are predominant in the early ranks of lineage trees, bRG-*apical-P* cells at intermediate ranks, whereas tbRG and IP cells are observed at the later ranks of division (Figure 6A). A similar but less pronounced trend is observed at E65 (Figure S4B).

Quantitative analysis of the progeny of each precursor type showed important qualitative and quantitative differences. All five precursor types are able to generate neurons and to self-renew, i.e., to generate at least one daughter of the same type as the mother cell. At both E65 and E78, we observed a self-renewal gradient, which is maximum in bRG-*both-P*, bRG-*apical-P*, and tbRG cells, intermediate in IP cells, and low in bRG-*basal-P* cells (Figure 6B). This suggests that the presence of the apical process is an important factor in conferring self-renewal properties to bRG cells.

The five precursor types exhibit different trends in their neurogenic capacity. At E78, bRG-*both-P* cells show the highest and IP cells the lowest proportions of neuronal progeny (Figure 6C). Variations in the neurogenic capacity of the different precursor types influence the size of their progeny. For instance, bRG-*both-P* and IP cells have comparable progeny (Figure 6D; Figure S4C), despite the fact that they are respectively at the top and bottom ranks of the lineage trees. The similarity in progeny of these two precursor types is due to the fact that IP cells have considerably lower neurogenic potential compared to bRG-*both-P* cells (Figure 6C).

The quantitative differences in the neurogenic potential and rates of self-renewal coupled with lineage rank suggest that different precursor types have distinct relationships. In order to investigate this, we developed a formal graphic description of the full repertoire of precursor behavior. In these state transition diagrams (Harel, 1987), nodes (or states) represent precursor types and directed edges the transitions between precursors (i.e., precursor progeny). Note that in state transition diagrams, each transition is expressed as a percentage of all transitions observed in the database and therefore is influenced by the frequency of each precursor type.

The state transition diagram formalizes statistically the hierarchical lineage relationships between the five precursor subtypes (Figure 6E). Of note, state transition analysis shows that precursors can transit bidirectionally between different types. At both stages and with only two exceptions, the downward transitions rates, going from low to high lineage ranks (i.e., down directed in the diagram), are stronger than upward transition rates.

At E65, average precursor ranks and precursor progeny variations are comparable to that observed at E78 (Figures 6A and 6D; Figures S4B and S4C). Interestingly, state transition diagrams are denser at E78 than at E65, with 28 out 30 possible transitions occurring versus 22 out of 30, respectively. The topology of the state transition graphs differs between the two stages in several salient ways. In particular, tbRG cells—which occur on average at rank 4 (Figure 6A) and represent the predominant precursor type generated at both stages by all precursors—are highly clustered with bRG-*apical-P* and IP cells via bidirectional transitions at E78. Interestingly, although tbRG cells have a much higher input at E78 than at E65, the frequency of tbRG cell transition to neurons does not change between the two stages. Instead, the increased tbRG cell output at E78 is characterized by new transitions to bRG-*apical-P* and bRG-*basal-P* cells as well as by an important strengthening of its transition to IP cells to which it becomes the strongest contributor. Because tbRG cells are characterized by both stronger inputs and outputs at E78 than at E65, they are endowed with a hub status at E78. IP cell production, self-renewal, and output are increased at E78 compared to E65.

All precursor types generate neurons with distinct frequencies. Neuron production is significantly higher for all precursor types at E65 than at E78. State diagrams reveal that bRG-*both-P* cells are the largest provider of neuronal progeny, followed by bRG-*apical-P*, tbRG, bRG-*basal-P*, and finally IP cells. These data show the existence of stage-specific differences in lineage relationships that result in precursor-specific differences in self-renewal, precursor pool amplification, and neuron production.

DISCUSSION

Technical Considerations

Compared to previous studies, our approach includes two major technical improvements. First, we have used an unbiased procedure to label cycling precursors, via retroviral infection. This

(H) Proportions of IP and bRG static morphology types in the OSVZ (four hemispheres, two slices per hemisphere, three GZ transects per slice).
(I) Quantification of the different static bRG morphotypes in the OSVZ (four hemispheres, two slices per hemisphere, three GZ transects per slice).
(J) Proportions of Pax6+ and/or Tbr2+ precursors in IP and bRG cell static morphology types in the OSVZ. ***$p < 0.001$ Fischer's exact test.
(K) Proportions of thick basal or apical processes in bRG-*both-P*, bRG-*basal-P*, or bRG-*apical-P*. Four hemispheres per stage, two to three slices per hemisphere, three GZ transects per slice. Mean ± SEM. *$p < 0.05$ Kruskal-Wallis test.
(L). Box-and-whisker plot of the length of basal and apical processes (basal process n = 396, apical process n = 339, four hemispheres, two to three slices per hemisphere, three GZ transects per slice). ***$p < 0.005$ Wilcoxon test.
(M) Percentages of bRG cells undergoing mitotic somal translocation (MST) toward the ventricle (downward) or toward the pia (upward) in the OSVZ.
(N) Example of a bRG undergoing an MST of 35 μm amplitude (cyan line) toward the ventricular surface in the ISVZ. Scale bar, 10 μm.
(O) Box-and-whisker plot of downward or upward MST amplitude. Not significant (NS) Wilcoxon test (downward n = 16, upward n = 16). See also Figure S2.

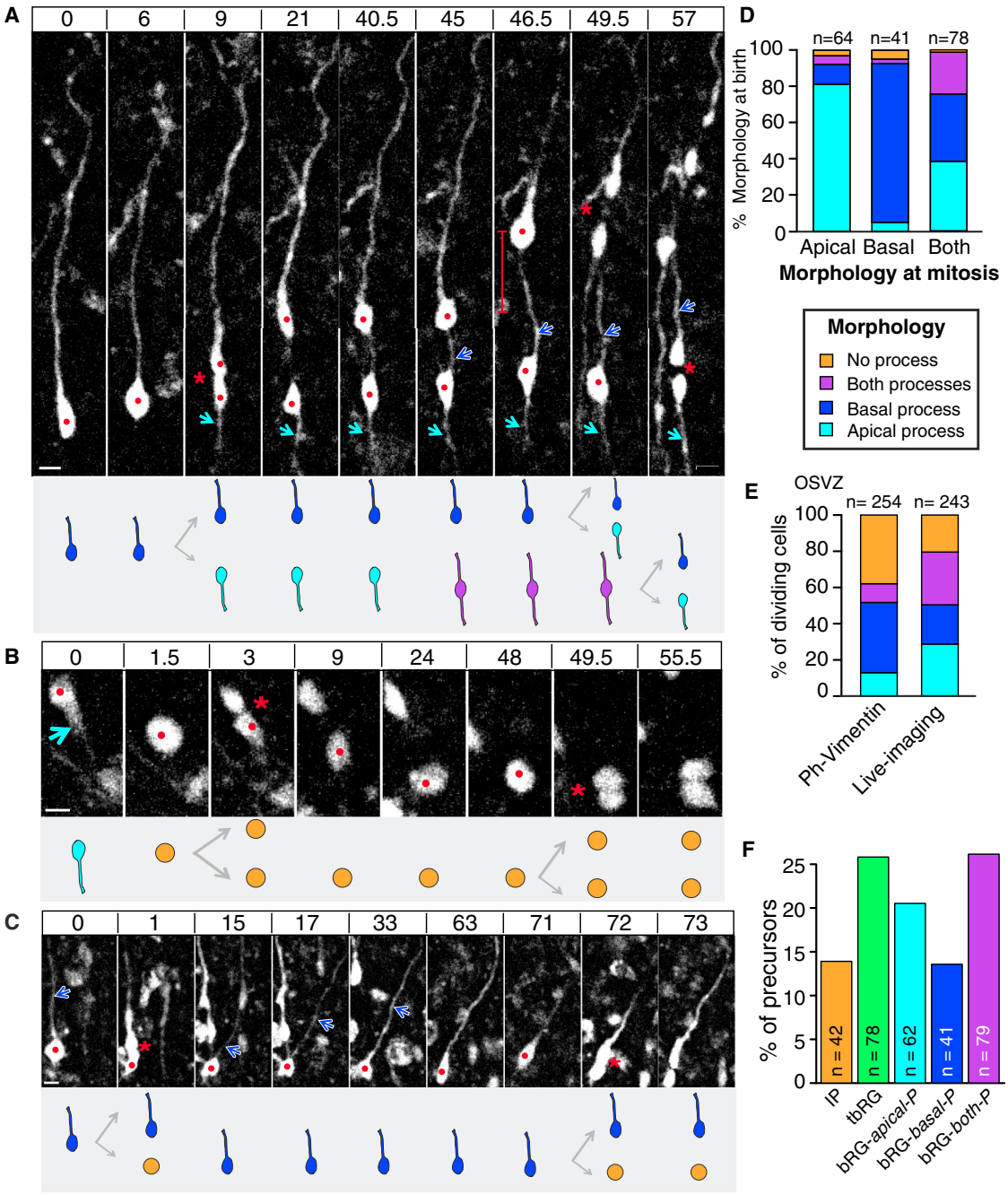

Figure 4. OSVZ Includes Five Precursor Types, with Stable and Dynamic Morphologies

(A–C) Selected images from TLV ex vivo recordings of GFP-retrovirus-labeled precursors showing stable or changing morphologies at E78 in the OSVZ. The images span the whole cell cycle (the lifetime) of the progenitor. The time at which the image was taken is indicated in hours. Progenitor morphology is schematized below each picture. Red dots indicate the cell under consideration, red stars divisions, dark blue arrowheads basal processes, and cyan arrowheads apical processes. Scale bars, 10 μm. (A) Example of bRG cells with a stable apical process (lower daughter) or a stable basal process (upper daughter). Note the MST of the upper daughter at t = 46.5 hr. (B) Example of an IP. (C) Example of a precursor born with no process that acquires a basal process 14 hr later. It is nonpolar for 20% of its lifetime and otherwise shows a bRG morphology and therefore corresponds to a transient tbRG.

(D) Correlation between the morphology observed in TLV at birth and at mitosis. The proportions of the morphologies at birth are represented according to the morphology at mitosis.

(E) Quantification of the morphology types at mitosis in the OSVZ as revealed by Ph-Vimentin staining or as observed in TLV observations of GFP+ precursors right before mitosis (8 hemispheres, 20 slices).

(F) Proportions of the five types of precursors identified in TLV (8 hemispheres, 20 slices). See also Figure S3.

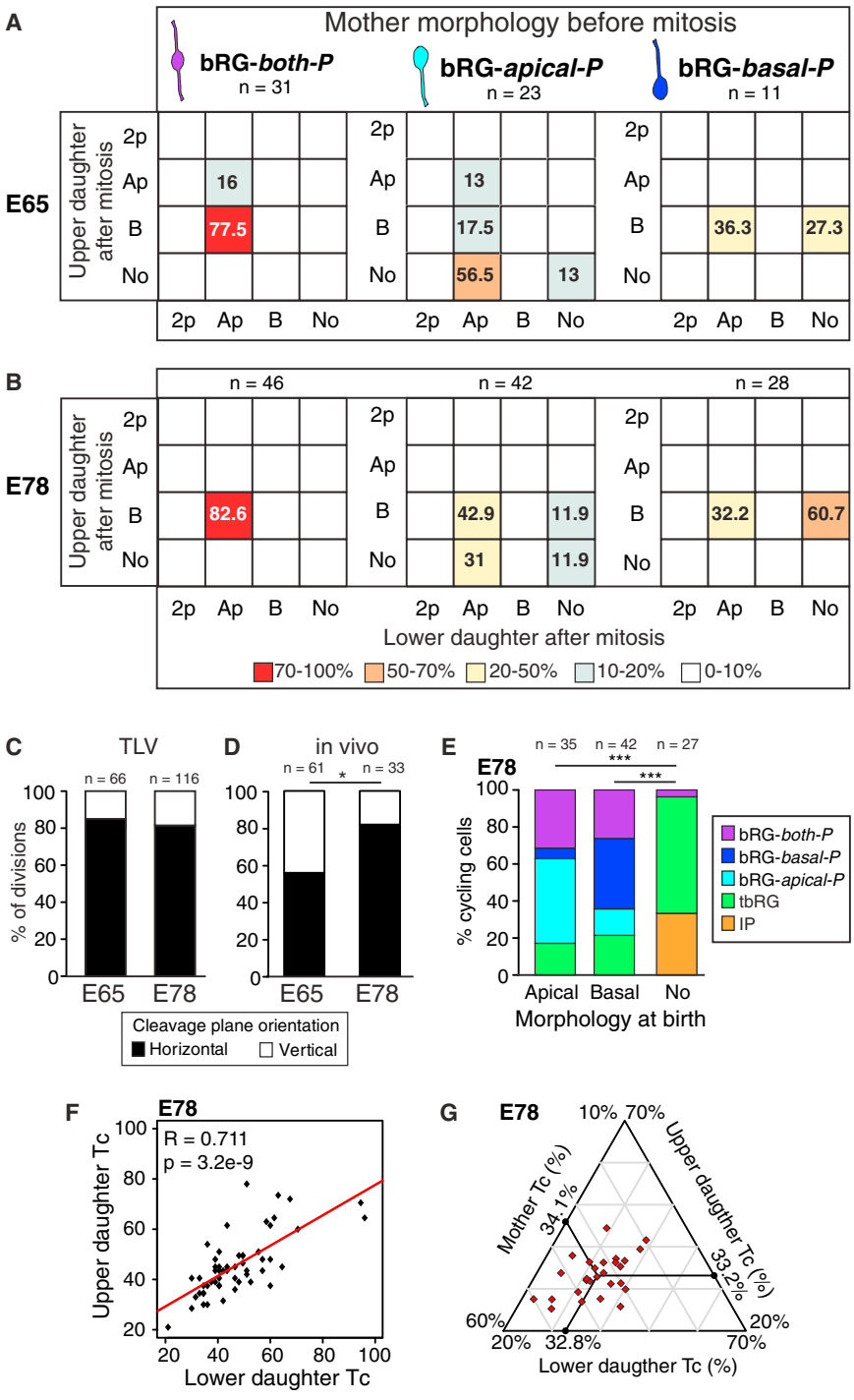

Figure 5. Rules of Process Inheritance and Link with Cell Fate

(A and B) bRG lower and upper daughter progeny varies with respect to the mother cell morphology before mitosis both at E65 (A) and E78 (B). Each table represents morphology frequencies of the paired daughter cells after mitosis with respect to bRG mother cell morphology before division. Row entry: upper daughter cell morphology; column entry: lower daughter cell morphology. Numbers correspond to percentages of occurrence of daughter cell morphology combination. Only values >10% are indicated. 2p, both processes (apical and basal); Ap, apical process; B, basal process; No, no process; four hemispheres, ten slices per stage.

(C and D) bRG cleavage plane orientation of OSVZ divisions quantified in TLV (C) and in situ (D). Horizontal cleavage plane: 0° to 45° angle relative to the ventricular surface; vertical cleavage plane: 45° to 90° angle. (C) Four hemispheres, ten slices at each stage. NS Fisher's exact test, (D) five sections at each stage. *$p < 0.05$ Fisher's exact test.

(E) Influence of the inheritance of a process at birth on the daughter proliferative fate at E78. Morphology at birth refers to the morphology of the daughter cells right after the division of the mother cell. The daughter cell can inherit an apical, a basal, or no process from the mother cell; four hemispheres, ten slices. ***$p < 0.001$ Fisher's exact test.

(F) Cell-cycle durations (Tc) of pairs of daughter cells are correlated (n = 55 pairs from four hemispheres, ten slices, Sperman rank correlation).

(G) Tc of lower and upper daughter cells shows a certain degree of synchronization with Tc of the mother cell at E78. For each triad (mother cells and its upper and lower daughters), the relative contribution of the Tc of each cell to the sum of the three Tcs was computed and displayed in the triangle plot. For instance, the relative contribution of mother cell Tc corresponds to mother Tc/(mother Tc + upper daughter Tc + lower daughter Tc). Black lines indicate the mean values for each triad cell type; 27 triads from four hemispheres, ten slices.

reveals a higher diversity of BP types (Figure 7A) than previously reported in human (Fietz et al., 2010; Hansen et al., 2010; LaMonica et al., 2013). We have identified five precursor categories and found that the previously reported bRG-*basal-P* cells and IPs account each only for 15% of the total precursor population. bRG-*both-P* and tbRG each represent 25% and bRG-*apical-P* 20% of the total population. The fact that previous human studies reported occasional OSVZ precursor cells bearing apical processes but failed to identify bRG-*apical-P* cells and bRG-*both-P* cells as major precursor types (Fietz et al., 2010; Hansen et al., 2010; LaMonica et al., 2013) is in most part due to the labeling technique used. Whereas the retroviral infection technique used here provides an unbiased sampling of cycling precursors, the retrograde labeling of bRG cells via placement of dye or adenovirus on the pial membrane (Fietz et al., 2010; Hansen et al., 2010; LaMonica et al., 2013) will uniquely label bRG-*basal-P* cells. Of note, we have been able to implement dual labeling of Pax6 and Tbr2 on single morphologically distinct precursor types, which has not been done in other studies. Contrary to previous claims, these transcription factors fail to qualitatively distinguish IPs versus bRG cells.

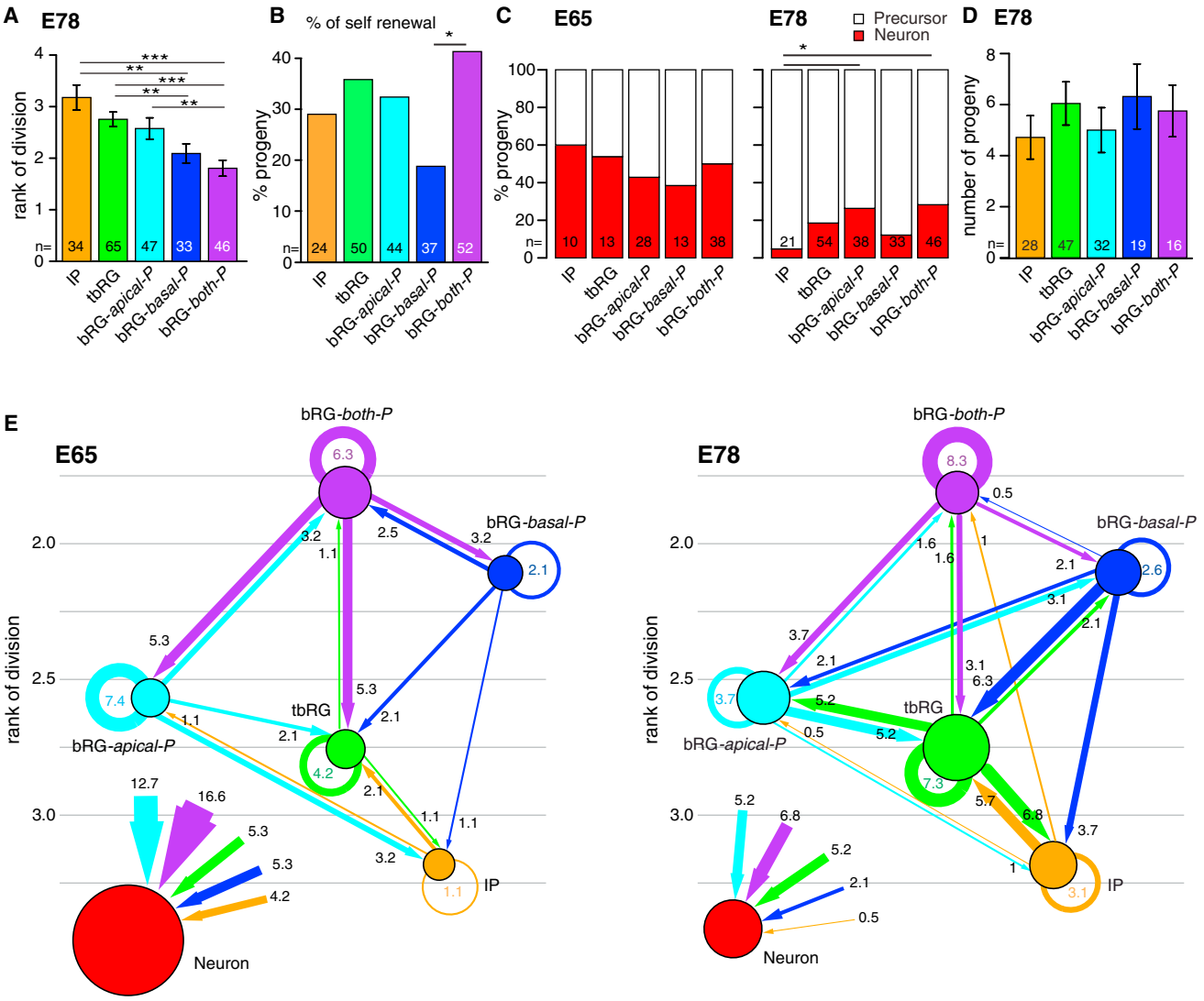

Figure 6. Progeny and Lineage Relationships between the Five Precursor Types

(A) Rank of each precursor type in the lineage trees at E78 (mean ± SEM, four hemispheres). **p < 0.01, ***p < 0.005 Wilcoxon test.

(B) Self-renewal of each precursor type (eight hemispheres). *p < 0.05 Fisher's exact test.

(C) Quantification of the neuronal versus proliferative progeny of the different precursor types at E65 and E78. *p < 0.05 Fisher's exact test.

(D) Histograms of the number of cells in the progeny of each precursor type (mean ± SEM, two hemispheres, three slices). NS Wilcoxon test.

(E) State transition diagrams illustrating the lineage relationships in OSVZ at E65 and E78. The diagrams consist of two components: nodes represent precursor types (states) and directed edges represent the transitions between precursors. There are a total of 30 possible transitions; from each of the five precursor types to the five precursor types (25 transitions) and to neurons (5). The size of the nodes is proportional to the frequency of each precursor type with respect to the total number of precursors and the thickness of the arrows to the frequency of each transition with respect to the total number of transitions. Numbers located near nodes indicate the transition frequency toward the node. The position of the nodes with respect to the vertical axis is determined by the mean rank of occurrence of each precursor type in the lineage trees (Figure 6D). Rank scale is indicated by light gray horizontal lines. The neurons have been extracted from the graph to ease the viewing of precursor's relationships. The size of the neuron nodes have been normalized with respect to the size of the samples at the two ages. E65: 34 lineage trees; 216 cells; 95 transitions. E78: 57 lineages trees; 479 cells; 192 transitions. (A–C and E) Data collected from four hemispheres, ten slices at each stage. See also Figure S4.

Second, we have been able to implement long-term live imaging of precursor behavior in the preserved environment of a cortical slice, as opposed to short-term observations reported in human tissue of reduced viability (LaMonica et al., 2013). This reveals that primate OSVZ precursors exhibit extensive proliferative abilities, undergoing up to six successive rounds of proliferative division. This long-term ex vivo assay provided an extensive and unique database of clonal observations of OSVZ precursor lineages, including key attributes of single precursor behavior (Tc, mode of division, direction of MST, upper or lower position at birth, size of progeny, self-renewal, and transitions). Quantitative analysis of this database makes it possible to

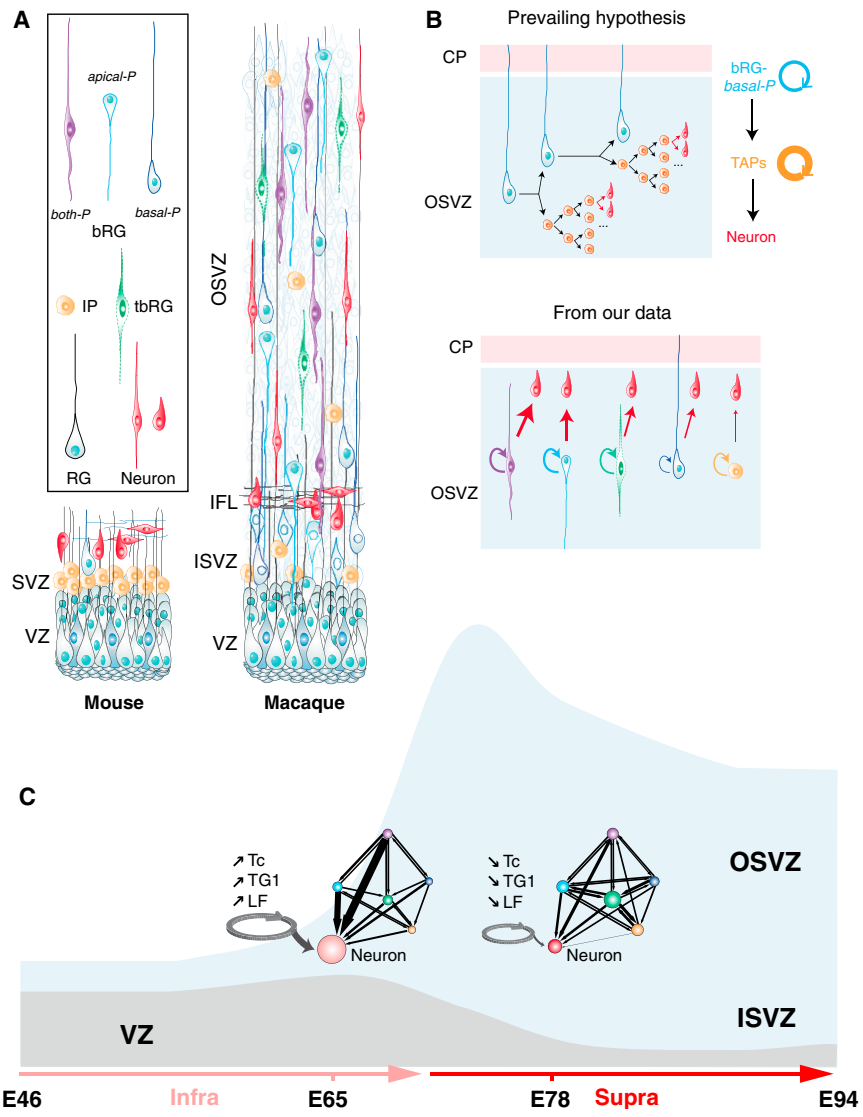

Figure 7. Model of Primate Corticogenesis

(A) Cartoon of the cell composition of the mouse and the macaque GZ. Note the scarcity of non-polarized IP in the macaque and the prevalence of radially oriented precursors bearing extensive apical and/or basal processes.

(B) Mode of OSVZ amplification. The prevailing hypothesis postulates that bRG-*basal-P* divide asymmetrically to generate a new bRG-*basal-P* and a transit amplifying cell (TAP), presumed to correspond to IP that undergoes several proliferative symmetric divisions before generating neurons (Lui et al., 2011). Here, we show that every precursor type self-renews and directly generates neurons, with however a varying contribution (proportional to the thickness of the red arrow).

(C) Stage-specific differences in cell-cycle parameters and lineage relationships of OSVZ precursors. Tc, cell-cycle exit and lineage relationship between OSVZ precursors vary between early and late stages of corticogenesis, corresponding to the generation of infra- and supragranular neurons, respectively. The shortening of Tc as well as the reduction of cell-cycle exit at later stages results in the amplification of the OSVZ precursor pool via multiple transitions between precursors. LF, leaving fraction which corresponds to cell-cycle exit.

extract precursor type-specific behavioral signature as well as to unravel the complex lineage relationships.

Specific Properties of OSVZ Precursors

The present study shows that macaque OSVZ progenitors exhibit several key morphological and behavioral characteristics of VZ RG cells. These include a radial glial morphology with basal and apical processes as well as extensive proliferative abilities. Like VZ RG cells, each of the five precursor types of the OSVZ is able to undergo symmetric proliferative divisions and to self-renew (Figures 6B–6D).

Of note, a fraction of bRG cells show precursor type-specific complex nuclear dynamics, reminiscent of interkinetic migration in RG cells in the VZ. In agreement with previous studies, we observe basally directed MSTs in bRG-*basal-P* cells (Hansen et al., 2010; LaMonica et al., 2012; Nelson et al., 2013). In addition, we observed apically directed MST and showed that bRG-*apical-P* exclusively undergo downward apical MST, while bRG-*basal-P* undergo exclusively upward basal MST. Proper nuclear positioning is thought to be critical to ensure sufficient transcriptional capacity as well as to minimize transport distances between the nuclei and the cytoplasm in elongated cells (Gundersen and Worman, 2013).

Our findings suggest that the inheritance of the apical process plays a significant role in conferring self-renewal properties to macaque bRG daughter cells. This contrasts with the mechanism reported in mouse cortical precursors in which the daughter cell is required to inherit the basal process in order to retain proliferative abilities (Shitamukai et al., 2011). Of note, OSVZ IPs that are devoid of basal process undergo numerous proliferative divisions and/or self-renew (Figure S4A; Movie S4), as opposed to mouse IPs that almost undergo uniquely symmetric neuronal terminal divisions (Huttner and Kosodo, 2005). Our results suggest that bipolar epithelial-like morphology may be an important feature for self-renewal since bRG-*both-P* show the highest self-renewal rates.

The detailed analysis of precursor divisions showed that bRG-*apical-P* and bRG-*basal-P* differ by their upper or lower position immediately after mitosis: bRG-*apical-P* correspond mostly to lower daughters and bRG-*basal-P* to upper daughters. Further, the analysis of the fate of paired daughter cells generated by bRGs revealed that the rule that has been described for asymmetric divisions in the mouse and zebrafish VZ (Alexandre et al., 2010)—whereby the lower cell becomes the neuron and the upper cell remains a progenitor—does not operate in

macaque OSVZ, in accordance with the nonprominent role of the basal process in maintaining self-renewal abilities. Among the five precursor types, bRG-*both-P* cells stand at the early rank of the lineages and generate large progenies. This is in agreement with the recently reported bipolar RG cell in the embryonic mouse ventral telencephalon shown to exhibit extensive capacity to generate progeny (Pilz et al., 2013).

A striking property of a fraction of OSVZ precursors revealed by our TLV observations is the structural repatterning of their cytoskeleton during their lifetime, which underlines the need to perform high-resolution exhaustive observations in order to detect the full repertoire of morphotypes. In particular, we uncovered the occurrence of tbRG cells, which alternate between stages showing one or two processes and stages with none during their lifetime.

Morphological Diversity of bRG Cells Provides the Basis for Dynamic Cell Interactions

The above observations point to the OSVZ being a zone enriched in dynamic basal and apical processes (Figure 7A) that may serve to sample the microenvironment stretching from the pia to the VZ, and thereby integrating signals from pre- and postmitotic cells as well as from fiber layers. Apical processes could be seen extending as far as the VZ without, however, reaching the ventricular surface, providing the substrate for novel transient cellular interactions between bRG cells and precursor cells from the ISVZ and the VZ (Nelson et al., 2013; Yoon et al., 2008). Basal processes can underlie interactions between cycling precursors and postmitotic neurons from the subplate and the cortical plate, which may subserve a feedback signal (Polleux et al., 2001). Filopodia were also occasionally observed, providing the basis for lateral interactions with cycling or differentiating neighbor cells via Notch-Delta signaling (Nelson et al., 2013; Shitamukai et al., 2011; Yoon et al., 2008).

Extensive Proliferative Abilities of OSVZ Precursors

The present study provides evidence that OSVZ precursors undergo numerous successive rounds of proliferative divisions, generating complex precursor lineage trees.

The balance between proliferative and differentiative divisions is key for OSVZ evolutionary expansion and therefore must be tightly controlled by both intrinsic and extrinsic mechanisms. Notch signaling (Hansen et al., 2010) and Beta integrin signaling relayed via the basal process (Fietz et al., 2010) have been shown to contribute to the control of OSVZ precursor proliferation. The present data show that OSVZ precursors exhibit sustained proliferative abilities, with cell-cycle parameters comparable to the RG cells of the VZ. By contrast with earlier studies predicting that OSVZ progenitors predominantly divide in an asymmetric, neurogenic manner (Fish et al., 2008), we observed that, although not anchored at the apical junctional belt and/or basal lamina, BP cells are nevertheless able to undergo numerous rounds of symmetric proliferative divisions that are ultimately finely controlled. This appears as a remarkable feature since loss of polarity or epithelial integrity and delamination from the epithelium have been shown to lead to uncontrolled proliferation in numerous tissues (Gómez-López et al., 2013; Lee and Vasioukhin, 2008). The OSVZ has been suggested to correspond to an extracellular matrix (ECM) component-enriched microenvironment (Fietz et al., 2012). There is evidence that ECM molecules bind to specific growth factors and morphogens and regulate their bioavailability, thereby providing a dynamic microenvironment for local integration of adhesive and growth factor signaling (Brizzi et al., 2012). The OSVZ therefore provides a niche, harboring signals controlling stemness, proliferation, and differentiation (Fietz et al., 2012; Marthiens et al., 2010), which are complemented by signaling from other precursors and/or progeny outside the OSVZ, presumably via the basal and apical processes.

Spatiotemporal Regulation of Cell-Cycle Parameters in OSVZ: A Regulatory Framework Underlying the Enlarged Supragranular Layer Compartment in the Macaque and Human Cortex

Examination of the timing of the macaque GZ suggested that high proliferative rates are required to maintain and amplify the OSVZ progenitor pool over the protracted period of supragranular neuron production in the macaque (Dehay and Kennedy, 2007; Lukaszewicz et al., 2005). Here, we have been able to extract cell-cycle durations and proliferative behavior of precursors, which show a developmental regulation that departs from what has been described in the rodent (Arai et al., 2011; Caviness et al., 1995; Reznikov and van der Kooy, 1995) in several respects. First, we observed a smaller difference (15%–7% at E65 and E78, respectively) in Tc between APs and BPs than has been reported in the mouse (30%) (Arai et al., 2011). Second, while rodent precursor global Tc has been shown to steadily increase during corticogenesis, we observed a shortening of Tc both in the VZ—in agreement with P. Rakic's findings (Kornack and Rakic, 1998)—and in the OSVZ.

This reduction in Tc, by means of a reduction in TG1 and to a lesser extent in TS (Figure 2I), is associated with an increase in proliferative divisions (Figure 2C) and a reduction of cell-cycle exit (Figure 2E), in agreement with the relationship between TG1 and the mode of division in cortical precursors (Pilaz et al., 2009). Combined, these two processes contribute to the expansion of the OSVZ precursor pool observed at midcorticogenesis (Figure 7C). Tc shortening and decrease in cell-cycle exit rates are observed simultaneously in OSVZ and VZ. However, whereas the OSVZ continues to expand, the VZ declines, which suggests that the OSVZ expansion may benefit from a sustained or increased seeding by VZ precursors (LaMonica et al., 2013). The VZ starts to expand at early stages, before the generation of the OSVZ (Rakic, 2009). The observed coordination between Tc regulation in VZ and OSVZ at late stages underlies the important role of the VZ in cortical expansion throughout corticogenesis.

Supragranular layer neurons are generated by the OSVZ (Lukaszewicz et al., 2005). Therefore, this expansion of the OSVZ pool via Tc shortening and decrease in cell-cycle exit accounts for the sustained production of supragranular neurons during the second half of corticogenesis. This leads to the postulation that these specific properties of macaque OSVZ precursors account for the expansion of the cortex and the supragranular layer enlargement that characterize this species as well as the human.

One can hypothesize that the fine regulation of the cell cycle, beyond its impact on the size of the progenitor pools, will also influence distinct transcriptional sequences in precursors that will in turn determine postmitotic transcriptional programs generating neuronal diversity (Molyneaux et al., 2007), as suggested by a recent study showing that the combinatorial temporal patterning of precursors is responsible for increasing diversity in *Drosophila* CNS (Bayraktar and Doe, 2013).

Cortical Neurons of the Primate Are Generated by a Mosaic of Precursor Subtypes via Stage-Specific Lineages

In addition to their capacity to undergo symmetric proliferative divisions, as well as to self-renew, each of the five precursor types is able to generate neurons at E65 and E78. This indicates that OSVZ precursors generate neurons destined for infragranular and supragranular layers (Dehay et al., 1993; Rakic, 1974).

The lineage relationships between the different OSVZ precursor types revealed by the state transition diagrams provide a model of cortical development that departs from the prevailing view in which bRGs produce TAPs—identified as IPs—which symmetrically amplify before producing neurons (Figure 7B) (Fietz and Huttner, 2011; Fietz et al., 2010; Kriegstein et al., 2006; Lui et al., 2011). We report frequencies of transitions at the total precursor population level (Figure 6E) as well as neurogenic transitions for individual precursor types (Figure 6C). Our study shows that, at the two stages examined, IPs are in fact the smallest provider of neuronal progeny, the largest provider being bRG-*both-P*, followed in order of importance by bRG-*apical-P*, tbRG, and bRG-*basal-P* cells.

State transition analysis of lineages provides an explicit graphic description of data obtained from numerous lineage trees and reveals complex relationships between OSVZ precursors. One salient characteristic of OSVZ precursor lineage is the occurrence of bidirectional transitions that depart from the classical unidirectional lineage genealogy, including that reported in rodent corticogenesis (Noctor et al., 2004; Qian et al., 1998; Tyler and Haydar, 2013). One can hypothesize that precursor diversity and their complex lineage relationships changing over time reflects a process that allows for the self-organization of the cortex (Kennedy and Dehay, 2012).

Although the basic module of five precursor types is present at E65 and E78, the state transition analysis shows that lineage relationships between precursors show stage-specific differences. Specifically, the present results reveal differences in the topology of lineage state transitions during the generation of infra- and supragranular layer neurons. This provides an innovative conceptual framework for understanding the mechanisms ensuring the ordered production of phenotypically distinct neuronal populations.

While it is generally agreed that the Old World macaque monkey is a valid model for understanding many features of the human brain, future comparative studies of a range of different members of the primate order and nonprimates will be necessary in order to better define primate-specific features.

Temporal changes in competence have been shown to contribute to the generation of distinct neuronal types in distinct numbers during corticogenesis by a common pool of precursors (Jacob et al., 2008; Qian et al., 1998). The present results show that, superimposed on these changes in temporal competence, there are modifications in lineage relationships that are consistent with the observed changes in cell-cycle parameters (Figure 7C). This would imply that the interplay of temporal competence and lineage state transition topology is a widespread developmental mechanism in the CNS (Ulvklo et al., 2012).

EXPERIMENTAL PROCEDURES

For numbers of animals, see Supplemental Experimental Procedures. For numbers of hemispheres, slices, and cells, see figure legends.

Animals

Fetuses from timed-pregnant cynomolgus monkeys (*Macaca fascicularis*, gestation period 165 days) were delivered by caesarian section as previously described (Lukaszewicz et al., 2005). All experiments were in compliance with national and European laws as well as with institutional guidelines concerning animal experimentation. Surgical procedures were in accordance with European requirements 2010/63/UE. The protocol C2EA42-12-11-0402-003 has been reviewed and approved by the Animal Care and Use Committee CELYNE (C2EA 42).

Organotypic Slice Culture and Retroviral Infection

Occipital poles of embryonic hemispheres were isolated and embedded in 3% low-melting agarose in supplemented HBSS at 37°C. We cut 300-μm-thick parasagittal slices in 4°C supplemented HBSS using a vibrating blade microtome (Leica VT1000 S). Slices were incubated in GMEM medium containing pCMV-EGFP retrovirus (1 to 5.10^5 pi/ml), for 2 to 3 hr at 37°C. Slices were then mounted on on laminin/poly-lysine-coated 0.4 μm Millicell culture inserts in a drop of type I collagen and cultured at 37°C, 7.5% CO_2, in 6-well plates in GMEM supplemented with 1% sodium pyruvate, 7.2 μM beta-mercaptoethanol, 1% nonessential amino acids, 2 mM glutamine, 1% penicillin/streptomycin, and 10% FCS.

Antibodies

Primary antibodies used were rabbit anti-Ki67 (Neomarker, 1:400), rabbit anti-Ki67 FITC conjugated (Neomarker, 1:100), mouse anti-NeuN (Milipore 1/100), mouse anti-Pax6 (DSHB, 1/1,000), rabbit anti-Tbr2 (Abcam 1/4,000), sheep anti-EOMES (R&D 1:800), chicken anti-GFP (Invitrogen, 1:1,000), rabbit anti-Geminin (Santa-Cruz, 1:400), and mouse anti-PCNA (Dako, 1/100).

Lineage Tree Reconstruction

We performed 6,003.3 hr (i.e., ~250 days) of recording in this study. Images were taken every 1 to 1.5 hr for up to 15 days. A cell was considered proliferative if it underwent division during the recording period. It was designated as a neuron if it started radial migration with typical migrating neuron morphology or when it was observed nondividing for a duration exceeding 1.5 times the average cell-cycle length of the zone and age under consideration (E48 > 67 hr, E65 > 101 hr and 108 hr, at E78 > 69 hr and 74 hr in the VZ and OSVZ, respectively). We examined 1,071 cells (56 cells at E48; 50 at E67; 71 at E75, two hemispheres; 335 at E65; 559 at E78, four hemispheres). We analyzed 487 divisions (22 at E48; 142 at E65; 31 at E67; 45 at E75; 247 at E78).

Statistical Analysis

Quantitative data are presented as the mean ± SEM from representative experiments. Statistical analyses were performed using the R software. The tests and the corresponding p values are indicated in the figure legends. For data involving proportions of small number of data points, the Fisher's exact test was used. Nonparametric statistical tests were preferred because the data did not follow a normal distribution. Wilcoxon test was performed for mean comparison, Kruskal-Wallis test for one-way ANOVA. $p < 0.05$ was considered statistically significant. The hierarchical clustering (Figure 1J) was performed using the factoMineR package of R (Lê et al., 2008).

SUPPLEMENTAL INFORMATION

Supplemental Information includes Supplemental Experimental Procedures, four figures, and five movies and can be found with this article online at http://dx.doi.org/10.1016/j.neuron.2013.09.032.

ACKNOWLEDGMENTS

We thank K. Knoblauch for invaluable and expert guidance in R statistics. We are grateful to M. Valdebenito, M. Seon, F. Piollat, and B. Beneyton for excellent animal care. We are indebted to N. Doerflinger, S. Zouaoui, P. Misery, and C. Lamy for technical assistance and to P. Giroud and J.P. Laigneau for help with the iconography. Administrative and logistic support from C. Nay, N. Kolomitre, and J. Beneyton is acknowledged. Financial support was from FP7 SECO grant (FP7-2007 ICT-216593), LABEX CORTEX (ANR-11-LABX-0042), and LABEX DEVweCAN (ANR-10-LABX- 061) of Université de Lyon, within the program "Investissements d'Avenir" (ANR-11-IDEX-0007) operated by the French National Research Agency (ANR).

Accepted: September 23, 2013
Published: October 16, 2013

REFERENCES

Alexandre, P., Reugels, A.M., Barker, D., Blanc, E., and Clarke, J.D. (2010). Neurons derive from the more apical daughter in asymmetric divisions in the zebrafish neural tube. Nat. Neurosci. *13*, 673–679.

Arai, Y., Pulvers, J.N., Haffner, C., Schilling, B., Nüsslein, I., Calegari, F., and Huttner, W.B. (2011). Neural stem and progenitor cells shorten S-phase on commitment to neuron production. Nat. Commun. *2*, 154.

Bayraktar, O.A., and Doe, C.Q. (2013). Combinatorial temporal patterning in progenitors expands neural diversity. Nature *498*, 449–455.

Brizzi, M.F., Tarone, G., and Defilippi, P. (2012). Extracellular matrix, integrins, and growth factors as tailors of the stem cell niche. Curr. Opin. Cell Biol. *24*, 645–651.

Bystron, I., Blakemore, C., and Rakic, P. (2008). Development of the human cerebral cortex: Boulder Committee revisited. Nat. Rev. Neurosci. *9*, 110–122.

Caviness, V.S., Jr., Takahashi, T., and Nowakowski, R.S. (1995). Numbers, time and neocortical neuronogenesis: a general developmental and evolutionary model. Trends Neurosci. *18*, 379–383.

Dehay, C., and Kennedy, H. (2007). Cell-cycle control and cortical development. Nat. Rev. Neurosci. *8*, 438–450.

Dehay, C., Giroud, P., Berland, M., Smart, I., and Kennedy, H. (1993). Modulation of the cell cycle contributes to the parcellation of the primate visual cortex. Nature *366*, 464–466.

Englund, C., Fink, A., Lau, C., Pham, D., Daza, R.A., Bulfone, A., Kowalczyk, T., and Hevner, R.F. (2005). Pax6, Tbr2, and Tbr1 are expressed sequentially by radial glia, intermediate progenitor cells, and postmitotic neurons in developing neocortex. J. Neurosci. *25*, 247–251.

Fietz, S.A., and Huttner, W.B. (2011). Cortical progenitor expansion, self-renewal and neurogenesis-a polarized perspective. Curr. Opin. Neurobiol. *21*, 23–35.

Fietz, S.A., Kelava, I., Vogt, J., Wilsch-Bräuninger, M., Stenzel, D., Fish, J.L., Corbeil, D., Riehn, A., Distler, W., Nitsch, R., and Huttner, W.B. (2010). OSVZ progenitors of human and ferret neocortex are epithelial-like and expand by integrin signaling. Nat. Neurosci. *13*, 690–699.

Fietz, S.A., Lachmann, R., Brandl, H., Kircher, M., Samusik, N., Schröder, R., Lakshmanaperumal, N., Henry, I., Vogt, J., Riehn, A., et al. (2012). Transcriptomes of germinal zones of human and mouse fetal neocortex suggest a role of extracellular matrix in progenitor self-renewal. Proc. Natl. Acad. Sci. USA *109*, 11836–11841.

Fish, J.L., Dehay, C., Kennedy, H., and Huttner, W.B. (2008). Making bigger brains-the evolution of neural-progenitor-cell division. J. Cell Sci. *121*, 2783–2793.

García-Moreno, F., Vasistha, N.A., Trevia, N., Bourne, J.A., and Molnár, Z. (2012). Compartmentalization of cerebral cortical germinal zones in a lissencephalic primate and gyrencephalic rodent. Cereb. Cortex *22*, 482–492.

Gómez-López, S., Lerner, R.G., and Petritsch, C. (2013). Asymmetric cell division of stem and progenitor cells during homeostasis and cancer. Cell. Mol. Life Sci. Published online June 15, 2013. http://dx.doi.org/10.1007/s00018-013-1386-1.

Götz, M., and Huttner, W.B. (2005). The cell biology of neurogenesis. Nat. Rev. Mol. Cell Biol. *6*, 777–788.

Gundersen, G.G., and Worman, H.J. (2013). Nuclear positioning. Cell *152*, 1376–1389.

Hansen, D.V., Lui, J.H., Parker, P.R., and Kriegstein, A.R. (2010). Neurogenic radial glia in the outer subventricular zone of human neocortex. Nature *464*, 554–561.

Harel, D. (1987). Statecharts: a visual formalism for complex systems. Sci. Comput. Program. *8*, 231–274.

Haydar, T.F., Ang, E., Jr., and Rakic, P. (2003). Mitotic spindle rotation and mode of cell division in the developing telencephalon. Proc. Natl. Acad. Sci. USA *100*, 2890–2895.

Huttner, W.B., and Kosodo, Y. (2005). Symmetric versus asymmetric cell division during neurogenesis in the developing vertebrate central nervous system. Curr. Opin. Cell Biol. *17*, 648–657.

Jacob, J., Maurange, C., and Gould, A.P. (2008). Temporal control of neuronal diversity: common regulatory principles in insects and vertebrates? Development *135*, 3481–3489.

Kelava, I., Reillo, I., Murayama, A.Y., Kalinka, A.T., Stenzel, D., Tomancak, P., Matsuzaki, F., Lebrand, C., Sasaki, E., Schwamborn, J.C., et al. (2012). Abundant occurrence of basal radial glia in the subventricular zone of embryonic neocortex of a lissencephalic primate, the common marmoset Callithrix jacchus. Cereb. Cortex *22*, 469–481.

Kennedy, H., and Dehay, C. (2012). Self-organization and interareal networks in the primate cortex. Prog. Brain Res. *195*, 341–360.

Kennedy, H., Douglas, R., Knoblauch, K., and Dehay, C. (2007). Self-organization and pattern formation in primate cortical networks. Novartis Found. Symp. *288*, 178–194, discussion 195–198, 276–281.

Konno, D., Shioi, G., Shitamukai, A., Mori, A., Kiyonari, H., Miyata, T., and Matsuzaki, F. (2008). Neuroepithelial progenitors undergo LGN-dependent planar divisions to maintain self-renewability during mammalian neurogenesis. Nat. Cell Biol. *10*, 93–101.

Kornack, D.R., and Rakic, P. (1998). Changes in cell-cycle kinetics during the development and evolution of primate neocortex. Proc. Natl. Acad. Sci. USA *95*, 1242–1246.

Kriegstein, A., Noctor, S., and Martínez-Cerdeño, V. (2006). Patterns of neural stem and progenitor cell division may underlie evolutionary cortical expansion. Nat. Rev. Neurosci. *7*, 883–890.

LaMonica, B.E., Lui, J.H., Wang, X., and Kriegstein, A.R. (2012). OSVZ progenitors in the human cortex: an updated perspective on neurodevelopmental disease. Curr. Opin. Neurobiol. *22*, 747–753.

LaMonica, B.E., Lui, J.H., Hansen, D.V., and Kriegstein, A.R. (2013). Mitotic spindle orientation predicts outer radial glial cell generation in human neocortex. Nat. Commun. *4*, 1665.

Lê, S., Josse, J., and Husson, F. (2008). FactoMineR: an R package for multivariate analysis. J. Stat. Softw. *25*, 1–18.

Lee, M., and Vasioukhin, V. (2008). Cell polarity and cancer—cell and tissue polarity as a non-canonical tumor suppressor. J. Cell Sci. *121*, 1141–1150.

Levitt, P., Cooper, M.L., and Rakic, P. (1981). Coexistence of neuronal and glial precursor cells in the cerebral ventricular zone of the fetal monkey: an ultrastructural immunoperoxidase analysis. J. Neurosci. *1*, 27–39.

Lui, J.H., Hansen, D.V., and Kriegstein, A.R. (2011). Development and evolution of the human neocortex. Cell *146*, 18–36.

Lukaszewicz, A., Savatier, P., Cortay, V., Giroud, P., Huissoud, C., Berland, M., Kennedy, H., and Dehay, C. (2005). G1 phase regulation, area-specific cell

cycle control, and cytoarchitectonics in the primate cortex. Neuron *47*, 353–364.

Marín-Padilla, M. (1992). Ontogenesis of the pyramidal cell of the mammalian neocortex and developmental cytoarchitectonics: a unifying theory. J. Comp. Neurol. *321*, 223–240.

Marthiens, V., Kazanis, I., Moss, L., Long, K., and Ffrench-Constant, C. (2010). Adhesion molecules in the stem cell niche—more than just staying in shape? J. Cell Sci. *123*, 1613–1622.

Martínez-Cerdeño, V., Noctor, S.C., and Kriegstein, A.R. (2006). The role of intermediate progenitor cells in the evolutionary expansion of the cerebral cortex. Cereb. Cortex *16*(*Suppl 1*), i152–i161.

Martínez-Cerdeño, V., Cunningham, C.L., Camacho, J., Antczak, J.L., Prakash, A.N., Cziep, M.E., Walker, A.I., and Noctor, S.C. (2012). Comparative analysis of the subventricular zone in rat, ferret and macaque: evidence for an outer subventricular zone in rodents. PLoS ONE *7*, e30178.

Molyneaux, B.J., Arlotta, P., Menezes, J.R., and Macklis, J.D. (2007). Neuronal subtype specification in the cerebral cortex. Nat. Rev. Neurosci. *8*, 427–437.

Nelson, B.R., Hodge, R.D., Bedogni, F., and Hevner, R.F. (2013). Dynamic interactions between intermediate neurogenic progenitors and radial glia in embryonic mouse neocortex: potential role in Dll1-Notch signaling. J. Neurosci. *33*, 9122–9139.

Noctor, S.C., Martínez-Cerdeño, V., Ivic, L., and Kriegstein, A.R. (2004). Cortical neurons arise in symmetric and asymmetric division zones and migrate through specific phases. Nat. Neurosci. *7*, 136–144.

Pilaz, L.J., Patti, D., Marcy, G., Ollier, E., Pfister, S., Douglas, R.J., Betizeau, M., Gautier, E., Cortay, V., Doerflinger, N., et al. (2009). Forced G1-phase reduction alters mode of division, neuron number, and laminar phenotype in the cerebral cortex. Proc. Natl. Acad. Sci. USA *106*, 21924–21929.

Pilz, G.A., Shitamukai, A., Reillo, I., Pacary, E., Schwausch, J., Stahl, R., Ninkovic, J., Snippert, H.J., Clevers, H., Godinho, L., et al. (2013). Amplification of progenitors in the mammalian telencephalon includes a new radial glial cell type. Nat. Commun. *4*, 2125.

Polleux, F., Dehay, C., Goffinet, A., and Kennedy, H. (2001). Pre- and post-mitotic events contribute to the progressive acquisition of area-specific connectional fate in the neocortex. Cereb. Cortex *11*, 1027–1039.

Pontious, A., Kowalczyk, T., Englund, C., and Hevner, R.F. (2008). Role of intermediate progenitor cells in cerebral cortex development. Dev. Neurosci. *30*, 24–32.

Qian, X., Goderie, S.K., Shen, Q., Stern, J.H., and Temple, S. (1998). Intrinsic programs of patterned cell lineages in isolated vertebrate CNS ventricular zone cells. Development *125*, 3143–3152.

Rakic, P. (1974). Neurons in rhesus monkey visual cortex: systematic relation between time of origin and eventual disposition. Science *183*, 425–427.

Rakic, P. (2009). Evolution of the neocortex: a perspective from developmental biology. Nat. Rev. Neurosci. *10*, 724–735.

Reillo, I., de Juan Romero, C., García-Cabezas, M.A., and Borrell, V. (2011). A role for intermediate radial glia in the tangential expansion of the mammalian cerebral cortex. Cereb. Cortex *21*, 1674–1694.

Reznikov, K., and van der Kooy, D. (1995). Variability and partial synchrony of the cell cycle in the germinal zone of the early embryonic cerebral cortex. J. Comp. Neurol. *360*, 536–554.

Shitamukai, A., Konno, D., and Matsuzaki, F. (2011). Oblique radial glial divisions in the developing mouse neocortex induce self-renewing progenitors outside the germinal zone that resemble primate outer subventricular zone progenitors. J. Neurosci. *31*, 3683–3695.

Smart, I.H., Dehay, C., Giroud, P., Berland, M., and Kennedy, H. (2002). Unique morphological features of the proliferative zones and postmitotic compartments of the neural epithelium giving rise to striate and extrastriate cortex in the monkey. Cereb. Cortex *12*, 37–53.

Stancik, E.K., Navarro-Quiroga, I., Sellke, R., and Haydar, T.F. (2010). Heterogeneity in ventricular zone neural precursors contributes to neuronal fate diversity in the postnatal neocortex. J. Neurosci. *30*, 7028–7036.

Tyler, W.A., and Haydar, T.F. (2013). Multiplex genetic fate mapping reveals a novel route of neocortical neurogenesis, which is altered in the Ts65Dn mouse model of Down syndrome. J. Neurosci. *33*, 5106–5119.

Ulvklo, C., MacDonald, R., Bivik, C., Baumgardt, M., Karlsson, D., and Thor, S. (2012). Control of neuronal cell fate and number by integration of distinct daughter cell proliferation modes with temporal progression. Development *139*, 678–689.

Wang, X., Tsai, J.W., LaMonica, B., and Kriegstein, A.R. (2011). A new subtype of progenitor cell in the mouse embryonic neocortex. Nat. Neurosci. *14*, 555–561.

Weissman, T., Noctor, S.C., Clinton, B.K., Honig, L.S., and Kriegstein, A.R. (2003). Neurogenic radial glial cells in reptile, rodent and human: from mitosis to migration. Cereb. Cortex *13*, 550–559.

Yoon, K.J., Koo, B.K., Im, S.K., Jeong, H.W., Ghim, J., Kwon, M.C., Moon, J.S., Miyata, T., and Kong, Y.Y. (2008). Mind bomb 1-expressing intermediate progenitors generate notch signaling to maintain radial glial cells. Neuron *58*, 519–531.